Journal of Fluorine Chemistry 129 (2008) 1173–1179

Contents lists available at ScienceDirect

Journal of Fluorine Chemistry

journal homepage: www.elsevier.com/locate/fluor

Fluorinated transition alumina with $Al_{2-x/3}O_{3-x}F_x$ compositions: Thermal, chemical, structural and morphological investigations

M. Gaudon [a,*], J. Majimel [a], J.-M. Heintz [a], M. Feist [b], D. Dambournet [a], A. Tressaud [a]

[a] Institut de Chimie de la Matière Condensée de Bordeaux, UPR 9048-CNRS, 87 Avenue du Docteur Schweitzer, 33608 Pessac, France
[b] Humboldt-University Berlin, Institute of Chemistry, Brook-Taylor-Str. 2, D-12489 Berlin, Germany

ARTICLE INFO

Article history:
Received 1 July 2008
Received in revised form 8 September 2008
Accepted 9 September 2008
Available online 20 September 2008

Keywords:
Alumina
AlF_3
Al–O–F
Oxide–fluoride

ABSTRACT

Fluorinated transition aluminas ($Al_{2-x/3}O_{3-x}F_x$) with hexagonal platelet shape were synthesized via decomposition of α-AlF_3 under air; they are thermally stable up to 1000 °C and exhibit at 1150 °C a weight loss with volume reduction caused by fluorine departure corresponding to a phase transition toward corundum alumina. The different characterizations performed in this study are structural (XRD), chemical (TGA-MS and microprobe analysis) and morphological (SEM, TEM and dilatometry). The evidence provided from this study is consistent with the formation of an Al–O–F phase as an intermediate compound in the pyrohydrolysis of an aluminium trifluoride phase to α-Al_2O_3.

1. Introduction

Numerous transition aluminas with different crystallographic forms are reported in the literature [1–5] as α, χ, γ, δ, η, κ phases, etc. For instance, the structure of γ-alumina has been described as having a cubic spinel structure with $Fd\bar{3}m$ symmetry but with tetragonal site distortion in the structure [6], the structure of the k-phase is also built of tetrahedral and octahedral sites but with a more complex feature [7], etc. These phases can be produced by the moderate annealing of various aluminium hydroxides minerals (gibbsite, boehmite, etc.). As illustration, the annealing at normal pressure of boehmite leads firstly to γ-Al_2O_3 (between 400 and 700 °C), then to δ-Al_2O_3 (700–1050 °C), θ-Al_2O_3 around 1050 °C and finally to α-Al_2O_3 over 1100 °C whereas bayerite annealing leads to the sequence η-Al_2O_3 (300–600 °C), θ-Al_2O_3 (800–1000 °C), α-Al_2O_3 (over 1000 °C) [8]. As far as the dehydration kinetically depends on the morphology-structure-composition of the starting aluminium hydroxide, a wide range of intermediate crystallographic alumina forms can thus be obtained depending on the rate and the atomic position of the residual hydroxyl groups. After total dehydration, all alumina forms finally transform into α-Al_2O_3, which is the thermodynamically stable phase.

Because the fluoride ion possesses to a first approximation the same size and the same charge as the hydroxyl ion, one could think that the decomposition of aluminium fluorides under air should occur via the successive formations of intermediate crystallographic phases. Apparently, that is not the case and no study has ever evidenced intermediate fluorinated alumina with $Al_{2-x/3}O_{3-x}F_x$ compositions. For instance, $AlF_{1.5}(OH)_{1.5}$ hydroxy-fluoride pyrochlore-type decomposes under nitrogen at 450 °C into two phases: α-AlF_3 aluminium fluoride and α-Al_2O_3 alumina. Moreover, the addition of fluorides (AlF_3, CaF_2, MgF_2, LiF, etc.) can be used in order to decrease the γ-Al_2O_3 → α-Al_2O_3 temperature transformation via the surface substitution of fluorine species for hydroxyl groups [9–12] but without bulk fluorination. Hence, it seems a priori difficult to get fluoride anions homogeneously dispersed into the anionic network of an "alumina". Nevertheless, due to the electronegativity of the fluorine element, numerous studies have been devoted to the surface fluorination of alumina with regard to the improvement of surface reactivity for catalytic applications. Two ways are generally used to prepare fluorinated alumina: (i) the use of gaseous fluorides or CFC reagents [13–18] and (ii) impregnation using a fluorinated aqueous solution (with NH_4F as impregnation agent) [19,20]. The first route leads to a reorganization of the alumina structure since α-AlF_3 [13], pyrochlore [16] phase and fluorides phase mixture [17,18] have been identified depending on the fluorination conditions. In the second route, for low fluorine contents, replacement of hydroxyl groups occurs mostly at the surface of alumina [19]. For higher

* Corresponding author.
E-mail address: gaudon@icmcb-bordeaux.cnrs.fr (M. Gaudon).

0022-1139/$ – see front matter © 2008 Elsevier B.V. All rights reserved.
doi:10.1016/j.jfluchem.2008.09.004

fluorine contents, X-ray diffraction has revealed the presence of α-AlF_3 phase [20]. The fluorination of alumina, whatever the way used, apparently has not led to the incorporation of fluoride ions inside the alumina networks.

An attempt of synthesizing aluminium oxide–fluoride compounds from the thermal decomposition of AlF_3 was performed and here reported. The thermal stability of aluminium fluorides has been generally investigated in an inert atmosphere avoiding any pyrohydrolysis process aiming for the identification of new fluoride phases [21] or phase transformations [22–24]. Therefore, to our knowledge, no investigation has dealt in detail with the thermal transformation of anhydrous AlF_3 under air atmosphere. Here, it has been isolated intermediate fluorinated aluminas, with a composition proximal to pure oxide alumina but with the presence of fluorine groups. These fluorine groups influence the obtained crystallographic structure, the morphology of the crystallites, their agglomeration, their chemical stability, etc.

2. Results and discussion

2.1. AlF_3 thermal decomposition

α-AlF_3 obtained from either synthesis route described in experimental section was calcined under air atmosphere at different temperatures ranging from 400 to 1200 °C. The chemical composition in fluorine and aluminium was determined using an electron probe for samples treated at different calcination temperatures. Changes in the F/Al molar ratio, relating to fluoride ions departure from the starting product are reported in Fig. 1.

The decomposition of the starting fluoride can be divided into three distinct zones. First, the α-AlF_3 appears to be stable up to 400 °C since a ratio F/Al equal to 3 is maintained in this range. Between 400 and 500 °C, α-AlF_3 decomposes into an aluminium oxide fluoride with a formula very close to Al_2O_3, the fluorine rate decreasing drastically to a F/Al molar ratio about 0.12 due to a pyro-hydrolysis process. In a second step, between 600 and 1000 °C, the fluorine remaining in the solid seems to be tightly inserted since after calcination at 1000 °C the F/Al molar ratio is still equal to 0.08. It is difficult to clearly settle from microprobe results only if along this calcination temperature range (600–1000 °C), whether there is a slight departure of fluorine versus temperature or a total stability of the fluorine content. One can assume that the microprobe analyses seem to indicate a continuous and weak defluorination. At last, in a third step, fluoride ions completely disappear after a sintering at 1200 °C and a fluorine-free alumina is obtained.

In Table 1, are collected together with F/Al molar ratios, the corresponding compositions with $Al_{2-x/3}O_{3-x}F_x$ formulation, considering no vacancies for the anionic network (i.e. three anions per formula). In other words, the substitution of one fluoride anion for an oxygen one is considered to yield the formation of 0.33 vacancy in the cationic network.

The structural evolution of the Al–O–F product was investigated by X-ray diffraction study. Patterns recorded for starting α-AlF_3 and for materials calcinated at 800 and 1200 °C under air atmosphere are reported in Fig. 2. After calcination at 800 °C, i.e. within the second step previously mentioned and corresponding to the presence of a low fluorine amount in the "oxide", all main diffraction lines can be indexed with a $P6_3mc$ Al_2O_3 cell (no. 26-0031 [4]); this phase is hereafter named κ-phase as it was already quoted in literature [25–27]. However, Al_2O_3 corundum form is detected as impurity. A more detailed investigation of the corundum to κ-phase ratio clearly shows that the corundum phase appears in larger and larger amounts with increasing temperatures. This trend suggests that the formation of corundum

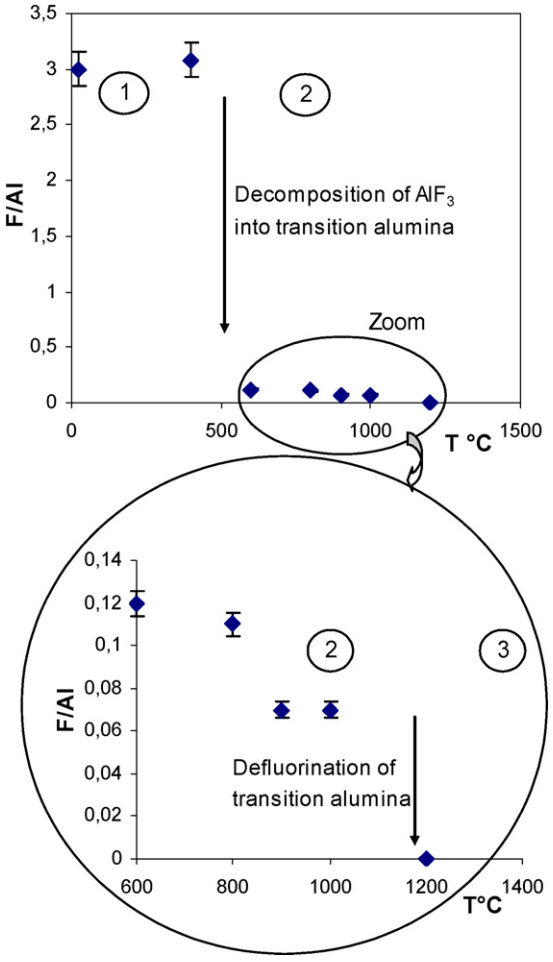

Fig. 1. Electron micro-probe results showing the F/Al ratios after α-AlF_3 burning at various temperatures (10 h calcinations under dry air of the starting α-AlF_3 product).

impurity can be associated with the slight fluorine departure observed with microprobe chemical analyses for calcinations temperature between 600 and 1000 °C. We propose that corundum formation starts at the surface due to this pyrohydrolysis phenomenon. Comparison of the FWHM of the peaks for the two phases clearly shows that the formation of the corundum phase is associated to a crystallite growth, the diffraction peaks of the corundum form being sharper than those of the κ allotropic form. Debye Sherrer calculation has shown indeed that the crystalline sizes of the latter do not exhibit any variation between 600 and 1000 °C: the crystallite sizes are evaluated to 24, 25, 22 and 25 nm, for 600, 800, 900 and 1000 °C, respectively. For the 1200 °C corundum form, the Debye Scherrer evaluation shows the crystallite size is over 100 nm.

Table 1
F/Al ratios and $Al_{2-x/3}O_{3-x}F_x$ corresponding compositions versus burning temperatures (10 h calcinations under dry air-atmosphere of the α-AlF_3 starting product).

Calcination T (°C)	F/Al ratio	Al2−x/3O3−xFx composition
400	3.08	AlF3
600	0.12	Al1.92O2.77F0.23
800	0.11	Al1.93O2.79F0.21
900	0.07	Al1.95O2.87F0.13
1000	0.07	Al1.95O2.87F0.13
1200	0	Al2O3

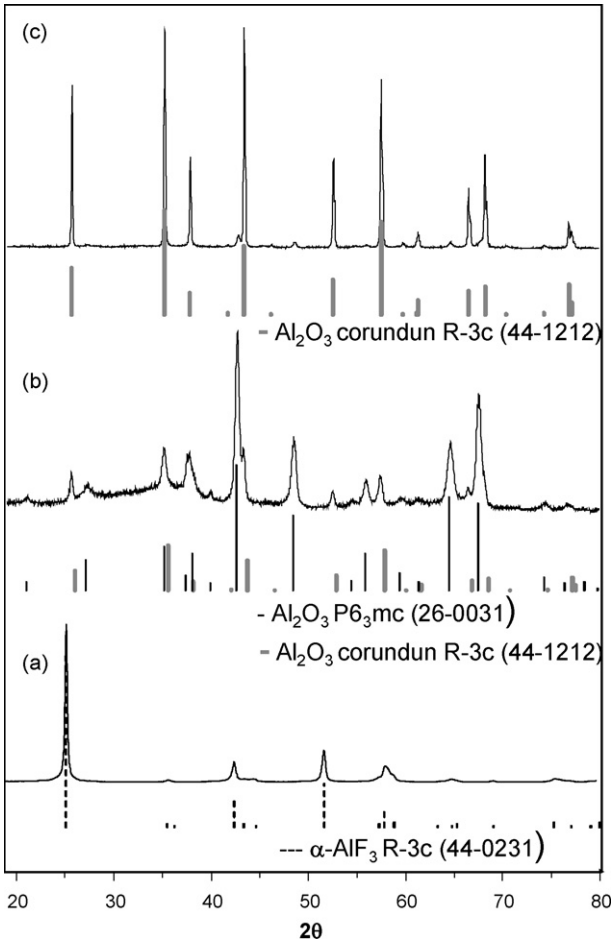

Fig. 2. XRD patterns: (a) for the starting AlF_3 product, (b) for the fluorinated transition alumina (obtained after α-AlF_3 burning at 1000 °C), (c) for the pure α-alumina form (obtained after α-AlF_3 burning at 1200 °C).

The correlation of the microprobe and XRD results, evidences that the presence of fluoride ions in small quantity in the Al–O–F product obtained after calcination under air at intermediates temperature ($600 \leq T \leq 1000$ °C) is responsible for the formation of fluorinated-alumina with the κ-form. Finally, the fluorine disappearance is accompanied by a sintering effect; that means that the presence of fluoride ions in the product inhibits the crystallite growth. At this point of the study, the sintering inhibitor effect can be directly associated with the presence of fluoride ions.

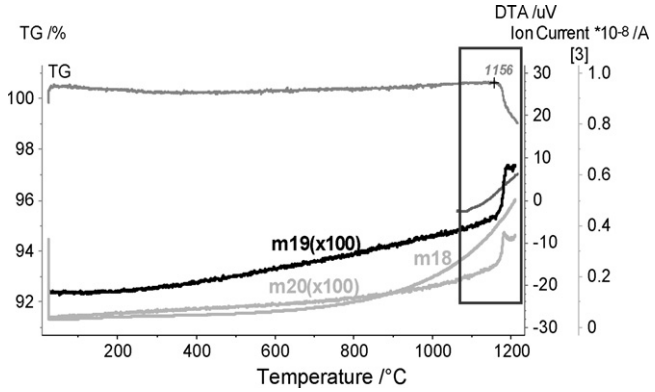

Fig. 3. Coupled TGA-MS analyses during a thermal treatment under air on the $Al_{2-x/3}O_{3-x}F_x$ powder obtained after α-AlF_3 pre-burning at 1000 °C.

2.2. Focus on $Al_{2-x/3}O_{3-x}F_x \rightarrow$ α-Al_2O_3 phase transformation

The second part of the study is focused on the transformation of the Al–O–F product with composition $Al_{1.95}O_{2.87}F_{0.13}$ obtained after calcination under air at 1000 °C into the corundum phase up to 1200 °C. Thermogravimetric and thermal differential analyses coupled with mass spectrometry (MS) were performed in this scope on the 1000 °C calcined-material as shown in Fig. 3.

No weight loss or drastic heat flow variation are detected in the large temperature range: room temperature to 1150 °C. Fluorine departure is determined through the ionic current of the fragments $m/z = 19$ (F^+) and 20 (HF^+). It should be noted that the continuous deviation of the MS base line of the fragments is due to the temperature-dependent intensity of the ionic current. Therefore, no gas departure is detected below 1100 °C. At about 1150 °C, the TGA curve exhibits a weight loss of 1.5–2% which is concomitant with the departure of fluorine detected through the $m/z = 19$ and 20 fragments. Moreover, identical curve shapes of both fragments unambiguously evidence the departure of HF since it confirms that the two fragments arise from the same molecule. Exothermic differential thermal flow seems to be associated to this gas departure. Note that the reaction $Al_{1.95}O_{2.87}F_{0.13} \rightarrow (-0.13\,F^- + 0.065\,O^{2-}) \rightarrow Al_{1.95}O_{2.93}$ would lead to a relative weight loss of 1.5%. TGA-MS analyses thus indicate that fluorine species present in the product seem to be abruptly

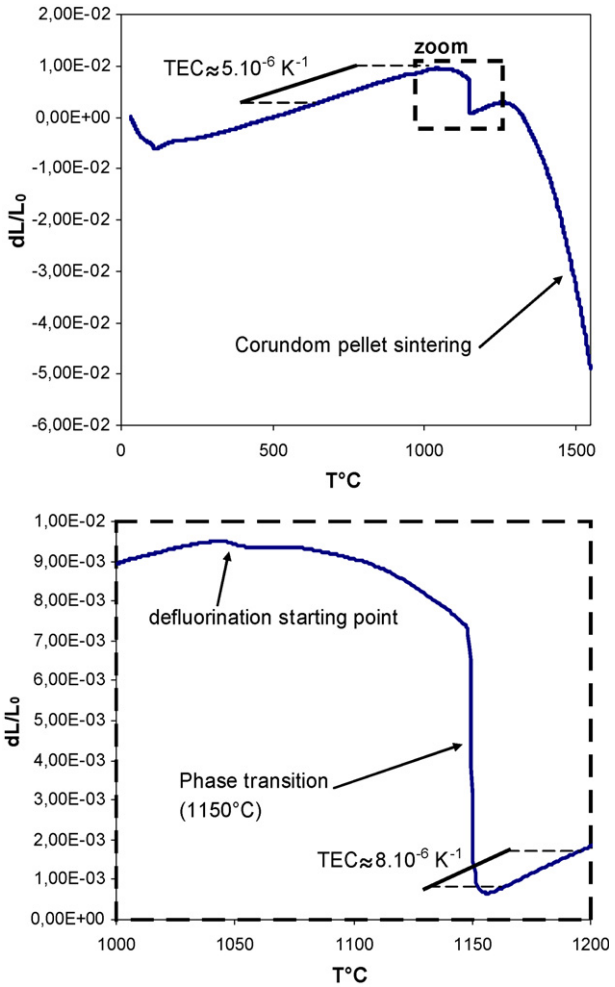

Fig. 4. Sintering curve of a pellet made of the $Al_{2-x/3}O_{3-x}F_x$ powder obtained α-AlF_3 pre-burning at 1000 °C.

replaced by half by oxygen ones at 1150 °C and, at such high temperature, whole the material (bulk and surface) should be concerned by the phenomenon.

The κ-phase to corundum phase transition is clearly linked the detected gaseous fluorine species. Although XRD at high temperatures would be the most suitable technique to confirm such assumption, the departure of very corrosive gaseous HF forbids the use of such technique. Hence, a dilatometric analysis was performed as an indirect way to confirm whether the fluorine departure is associated to the κ-$Al_{1.95}O_{2.87}F_{0.13}$ to corundum phase transition.

The sintering curve of the $Al_{1.95}O_{2.87}F_{0.13}$ pellet (calcined at 1000 °C) exhibits several steps (Fig. 4). The first shrinkage between room temperature and 150 °C corresponds to the oil surfactants used to obtain a mechanically stable pellet. Then, between 200 and 1150 °C the pellet expends with a thermal expansion coefficient which can be estimated roughly about 4–6 × 10^{-6} K^{-1}; very low expansion accounts for great bonds rigidity. This high bonds rigidity is due to very short and ionic bonds from the presence of fluoride ions. Then, a brutal shrinkage occurs around 1150 °C. In regard of the previous thermal analyses, it can be assumed to be associated with the κ-phase to corundum phase transition. This phase transition is followed by the expansion of the material with a thermal expansion coefficient about 7–8 × 10^{-6} K^{-1} corresponding to α-Al_2O_3 one. Finally, at 1250–1300 °C the sintering of the pellet starts. This sintering occurs at higher temperature than for a standard corundum pellet, may be because of the particular morphology of the corundum issued from the fluorinated κ-form here synthesized.

2.3. Morphology investigations of κ-$Al_{2-x/3}O_{3-x}F_x$ α-Al_2O_3 phases

In the last part the particular morphology of the κ-phase obtained between 800 and 1000 °C, and the morphology of the corundum form issued from this κ-phase after calcination at 1200 °C are both investigated.

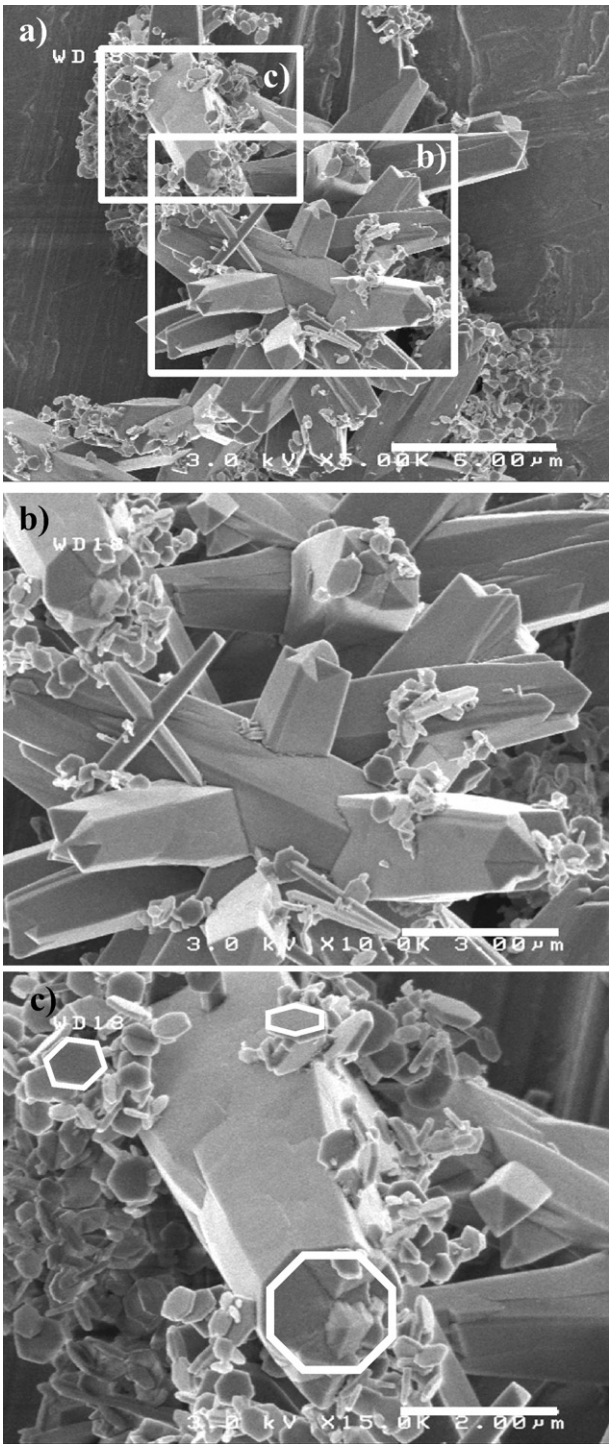

Fig. 5. SEM micrographs of the 1000 °C-calcined $Al_{2-x/3}O_{3-x}F_x$ agglomerates without sonication.

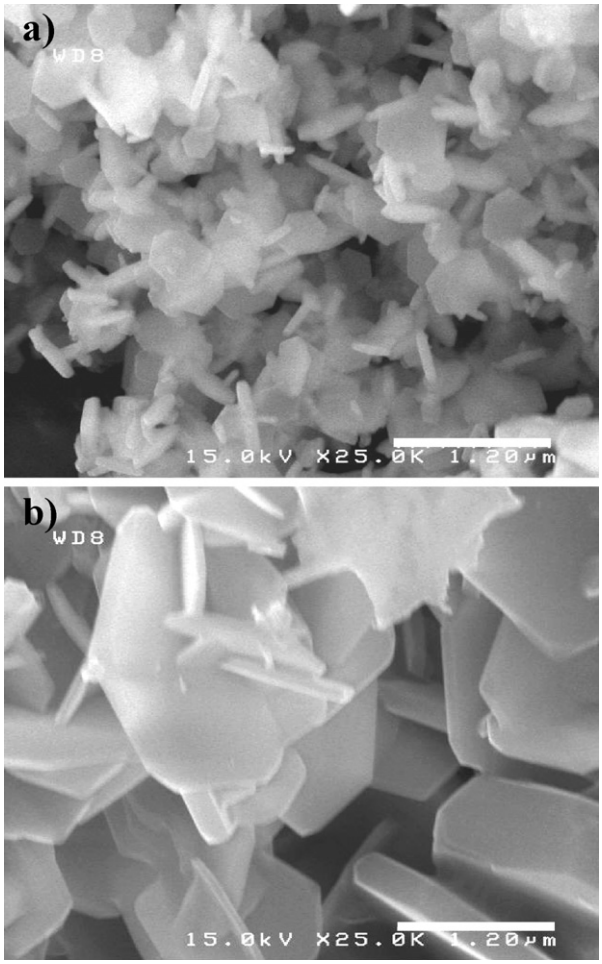

Fig. 6. SEM micrographs of 900 °C-calcined $Al_{2-x/3}O_{3-x}F_x$ crystallites (a) α-Al_2O_3 obtained after annealing at 1200 °C (b).

After calcinations of the α-AlF_3 raw product under air at 1000 °C, the κ-phase exhibits two distinct morphologies: (i) small "particles" presenting the shape of hexagonal platelets, (ii) big octagonal sticks. These two kinds of objects can be easily distinguished on the micrography reported in Fig. 5. The octagonal seem to be formed from the aggregation of the hexagonal platelets. These very coherent aggregates may be the cause of the noted delay of sintering of the alumina formed. Moreover, it can be noticed that after ultra-sonication in water, the sticks totally explode into hexagonal platelets as shown in SEM pictures reported in Fig. 6 for powders heat treated at 900 and 1200 °C, respectively. Some image analyses performed with the software ImageTool have allowed approximating the thickness (t) and the "diameter" (∅) of the hexagonal platelets: $t \leq 0.1$ μm, ∅≈0.4–0.5 μm and $t \approx 0.05$–0.3 μm, ∅≈2 μm, for 900 and 1200 °C calcination temperatures, respectively. The important point is the unambiguous conservation of the hexagonal platelet shape before and after the phase transition. The grain growth is roughly isotropic, the thickness/diameter ratio remaining quite constant. TEM analyses were then performed in order to get some crystallographic information from electronic diffraction patterns. It was brought to the fore that all the hexagonal platelet shape is due to a crystallographic six-order axis, as shown in TEM diffraction patterns (inset of Fig. 7a). It was furthermore observed that when the crystallites were maintained under the TEM electron beam, they partially melted (Fig. 7b) and recrystallized into a multitude of nano-fragments conserving a pseudo-hexagonal morphology (Fig. 7c) for which no crystallographic informations can be extracted. It can be nevertheless assumed that the fluorine departure should be at the origin of the crystallite evolution observed under electron beam.

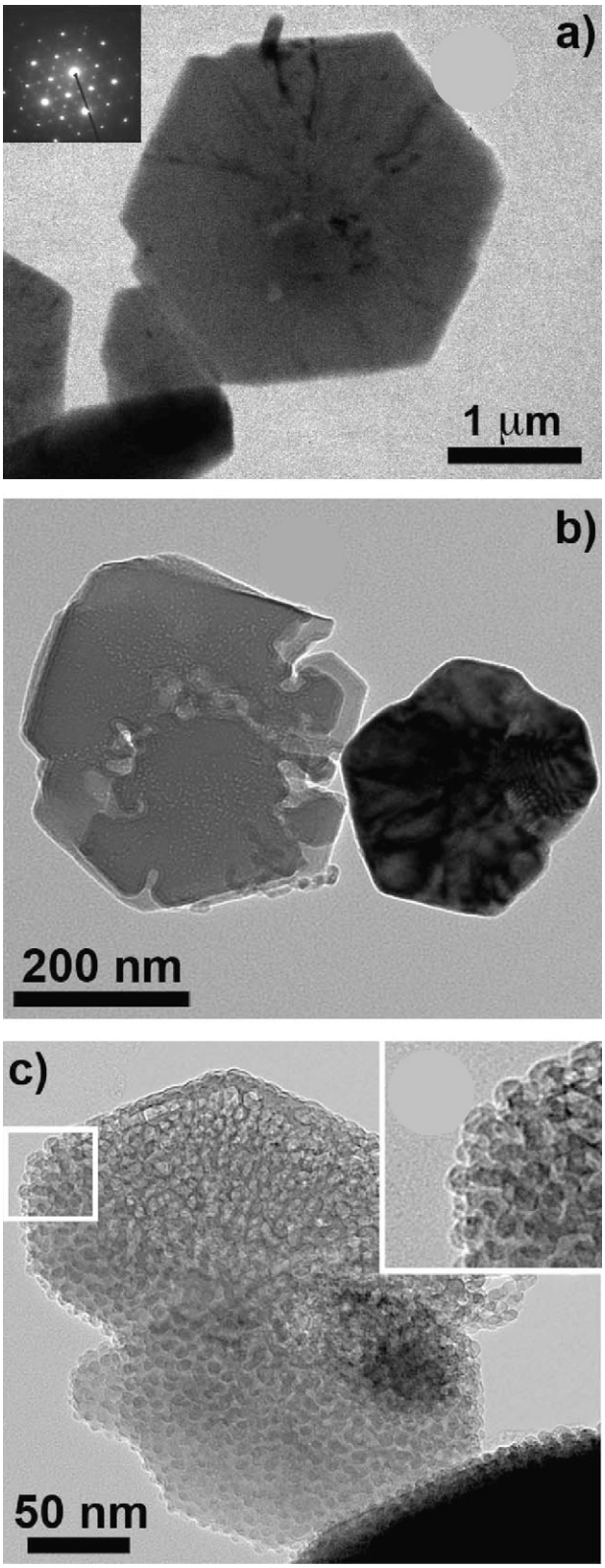

Fig. 7. TEM micrographs on the 1000 °C-calcined $Al_{2-x/3}O_{3-x}F_x$ crystallites (a), partial melting of the crystallite under the electron beam (b), followed by a recrystallisation of nano-crystallites (c).

These results open the window for many applications. As first example, transition aluminas being promising materials as catalysers, the enhancement of the catalytic activity could be achieved through the insertion inside the alumina network of fluorine groups in a sense that Lewis acidity of the cationic site is increased with the bond polarisation. In such a scope, the possibility of fluoride ions insertion into transition aluminas and the high thermal stability of the incorporated fluoride ions are important issues. As another example, the presence of fluoride ions inside the alumina matrix can influence upon the sintering mechanisms and thus, allow the morphological control of the α-Al_2O_3. Fluorine groups seem to hinder the sintering phenomenon, whereas one could have expected that the fluorine acts as a mineralizing additive in respect with previous literature works on the influence of fluorides additive on the Al_2O_3 corundum sintering [10–12]. The addition of fluorine can *a priori* preserve the porosity of porous alumina membranes submitted to high temperatures.

3. Conclusion

It was shown in this paper that fluorinated transition alumina, rich in oxygen and poor in fluoride anions, are formed during the decomposition process of α-AlF_3 under air atmosphere over 800 °C and which are stable up to 1150 °C. Indeed, at this last temperature, the weight loss measured by TGA is due to fluorine departure as shown by MS. A subsequent densification deduced by dilatometric analysis leads suddenly to the formation of corundum alumina. Hence, the alumina κ-type form observed before this decomposition temperature is without any doubt stabilized because of the participation of fluoride ions into the crystallographic network. For the first time an Al–O–F phase is so evidenced. In the second part of the study, the morphologic characterizations were performed. An interesting observation was made by TEM: even if this phase was synthesized at high temperature, it reveals itself unstable under the TEM beam probably due to fluorine departure.

4. Experimental

4.1. Synthesis routes

Several synthesis routes can be employed for the elaboration of highly divided α-AlF_3 aluminium fluoride material. Two of these routes are described below:

(i) from hydro-condensation in alcoholic media (ethanol) of aluminium propoxide (solid powder, Sigma–Aldrich) or tri-sec-butoxide (liquid, Sigma–Aldrich in butanol –97 wt%), with water/aluminium and HF/aluminium molar ratios equal to 5 and 3, respectively. The hydro-condensation leads to the formation of a colloidal sol and the sol–gel transition point is easily reached thanks to a partial drying performed of a hot sand bank. The obtained gel can be heated about 100 °C inside an oven in order to get a white amorphous xerogel; thereafter, highly divided α-AlF_3 is synthesized from calcination at 400 °C for 10 h, under air of this xerogel.

(ii) from precipitation under solvothermal conditions of an hydroxy-fluoride obtained from an aluminium salt and HF in an autoclave. In a first step, a precursor solution containing Al(III) chloride (Sigma–Aldrich 98% $AlCl_3{\cdot}9H_2O$) is prepared by dissolution in a water/isopropanol (1/1) solution. An aqueous solution of HF (Panreac, 40 wt%) is then added in order to get a HF/Al precursor molar ratio equal to 3.5. This solution is placed in a PTFE container for a microwave solvothermal treatment at 170 °C for 1 h. Thereafter, a powder is recovered by microwave-assisted drying performed under primary vacuum and argon flow. The as-prepared sample which consists of a divided hydroxy-fluoride is post-fluorinated in static condition using diluted F_2 (90% Ar) at 550 °C. This latter route leads to a pure crystalline phase, whereas the first one leads to a noticeable amorphous part besides the crystalline AlF_3 one.

Whatever the route used, the study of the thermal evolution under dry-air atmosphere of the resulting AlF_3 was performed by successive annealing at 400, 600, 800, 900, 1000 and 1200 °C with each time, a dwell at the required temperature of 10 h.

Some slight differences in the behaviour of the phase mixtures are obtained depending on the AlF_3 precursor: κ-Al–O–F phase crystallizes with the two synthesis routes used before the formation of α-Al_2O_3; nevertheless, the kinetic of its crystallization and transformation into α-alumina differs a bit. It evidences that the morphology (grain size, homogeneity, presence of surface water, etc.) of the starting α-AlF_3 precursor gets an influence. Herein this publication, we choose to expose only the results obtained with the α-AlF_3 precursor issued from the first (sol–gel) route.

4.2. Chemical analyses

Elemental composition was determined by means of a Castaing microprobe CECAMA SX 630 apparatus by Wavelength Dispersive Spectrometry. Analyses were performed on uniaxially pressed powdered pellets and yielded the relative Al/F molar ratio. Oxygen content was deduced to insure the right charge balance, the oxidation states of aluminium and fluorine being taken equal to III and –I, respectively. Each microprobe analyses were repeated three times on three distinct zones. Relative error bars on each composition measurement were calculated from standard deviation and tend to be less than 1% for alumina and 3% for fluorine rates. Furthermore, it has to be specified that the analyses were performed with a very large probe size of 100 μm^3 volume, ensuring thus a strong index of confidence for each measurement.

4.3. Structural investigations

X-ray diffraction (XRD) measurement was carried out at room temperature in the $20^\circ \leq 2\theta \leq 120^\circ$ range (step 0.017°) on a PANalytical X'PERT PRO diffractometer equipped with X'Celerator detector mounted in Bragg–Brentano scattering geometry. CuKα (Kα1–Kα2) radiation was used as X-Ray source.

4.4. Thermogravimetric analyses (TGA/MS)

Thermogravimetric analyses (TGA/MS) was performed using a NETZSCH thermoanalyzer STA 409 C *Skimmer*®. The thermoanalytical curves (T, DTA, TG, DTG) were recorded together with the ion current (IC) curves in the multiple ion detection (MID) mode for mass spectroscopies analyses. A constant purge gas flow of 70 mL/min nitrogen (N_2 5.0, Messer–Griesheim) and a constant heating rate of 10 K min^{-1} were applied.

4.5. Dilatometric analyses

Thickness variation versus temperature of $Al_{2-x/3}O_{3-x}F_x$ green pellet was recorded on a Netzsch DIL 402C dilatometer. The dilatometer is constituted of a horizontal furnace, contactors in alumina and displacement sensor. The acquisition system allows recording the total variation of the pellet sample and the contactors for which a correction is added in order to deduce the thickness relative variation ($\Delta L/L_0$) of the only sample. The pellet is elaborated by the application of uniaxial pressure on 1000 °C-calcined $Al_{2-x/3}O_{3-x}F_x$ powder. The technique is used to extract information on the sintering steps (temperatures, association with expansion or contraction, quantification of the expansion/shrinkage, etc.).

4.6. Microscopies

(i) For scanning electronic microscopy (SEM) analysis, we used a field effect gun-scanning electronic microscope (FEG-SEM) in order to characterize the crystallite as well as the crystallite morphology (shape, size and special rearrangement) on which the spatial resolution can be estimated about 1 nm.

(ii) Transmission electronic microscopy (TEM) was performed on a TECNAI F20 equipment with a field emissive gun, operating at 200 kV and with a point resolution of 0.24 nm. TEM samples were prepared by dissolving few milligrams of powder in ethanol. The solution was then dipped ten minutes into an ultrasonic bath in order to disagglomerate and disperse powder particles. One drop of the solution was finally deposited on a Formvar/Carbon copper grid.

Acknowledgments

The EU is acknowledged for financial support through the 6th Framework Programme (FUNFLUOS, Contract No. NMP3-CT-2004-5005575).

References

[1] A.G. Belogrudov, N.I. Permikina, D.S. Rutman, L.N. Shmuilov, A.V. Mytnikov, N.Z. Nasyrov, Refractories (English translation of Ogneupory) 24 (3–4) (1983) 211–214.
[2] N.M. Permikina, D.S. Rutman, A.V. Mytnikov, N.I. Gorbachev, P.I. Vol'pin, I.I. Panasenko, E.S. Butovskaya, D.B. Min'kov, N.S. Logacheva, B.V. Parkhaev, V.P. Ryabov, Refractories 19 (5–6) (1978) 345–352.
[3] E.J.W. Verwey, Zeitschrift fuer Kristallographie, Kristallgeometrie, Kristallphysik, Kristallchemie 91 (1935) 317–320.
[4] M. Okumiya, G. Yamaguchi, Bulletin of the Chemical Society of Japan 44 (1971) 1567–1570.
[5] Y. Repelin, E. Husson, Material Research Bulletin 25 (1990) 611–621.

[6] G. Paglia, C.E. Buckley, A.L. Rohl, B.A. Hunter, R.D. Hart, J.V. Hanna, L.T. Byrne, Physical Review B—Condensed Matter and Materials Physics 68 (2003) 1441101–14411011.
[7] G. Paglia, A.L. Rohl, C.E. Buckley, J.D. Gale, Journal of Material Chemistry 11 (2001) 3310–3316.
[8] B.C. Gates, J.R. Katzer, G.C.A. Schuit, Chemical Engineering Series, McGraw Hill, 1979
[9] J.L. Fourquet, M. Riviere, A. Le Bail, M. Nygrens, J. Grins, European Journal of Solid State Inorganic Chemistry 25 (1988) 535–545.
[10] Z. Zivkovic, N. Strbac, J. Sestak, Thermochimica Acta 266 (1995) 293–300.
[11] Y. Wu, Y. Zhang, G. Pezzoti, J. Guo, Materials Letter 52 (2002) 366–369.
[12] I. Ganesh, S. Bhattacharjee, B.P. Saha, R. Johnson, Y.R. Mahajan, Ceramics International 27 (2001) 773–779.
[13] P.J. Chupas, M.F. Ciraolo, J.C. Hanson, C.P. Grey, Journal of the American Chemical Society 123 (2001) 1694–1702.
[14] P.J. Chupas, D.R. Corbin, V.N.M. Rao, J.C. Hanson, C.P. Grey, Journal of Physical Chemistry B 107 (2003) 8327–8336.
[15] P.J. Chupas 1, C.P. Grey, Journal of Catalysis 224 (2004) 69–79.
[16] J.M. Saniger, N.A. Sanchez, J.O. Flores, Journal of Fluorine Chemistry 117 (1998) 88.
[17] T. Skapin, Journal of Materials Chemistry 5 (1995) 1215–1222.
[18] T. Skapin, E. Kemnitz, Catalytic Letters 40 (1996) 241–247.
[19] L. Fischer, V. Harlé, S. Kasztelan, J.-B. d'Espinose de la Caillerie, Solid State Nuclear Magnetic Resonance 16 (2000) 85–91.
[20] W. Zhang, M. Sun, R. Prins, Journal of Physical Chemistry B 106 (2002) 11805–11809.
[21] H. Norman, W.E. Farneth, Advanced Materials 8 (1996) 959.
[22] C. Alonso, A. Morato, F. Medina, F. Guirado, Y. Cesteros, P. Salagre, J.E. Sueiras, A. Giralt, Chemistry of Materials 12 (2000) 1148–1155.
[23] D.H. Menz, A. Zacharias, L. Kolditz, Journal of the Thermal Analysis 33 (1988) 811–815.
[24] M. Feist, E. Kemnitz, Thermochimica Acta 446 (2006) 84–90.
[25] H.C. Stumps, A.S. Russel, J.W. Newsome, C.M. Tucker, Industrial and Engineering Chemistry 42 (1950) 1398.
[26] E. Kemnitz, D.H. Menz, Progress in Solid State Chemistry 26 (1998) 97.
[27] B.C. Lippens, J.H. De Boer, Acta Crystallographica 17 (1964) 1312.